Oxygen Reduction Reaction

International Edition: DOI: 10.1002/anie.201601727
German Edition: DOI: 10.1002/ange.201601727

Theoretical Modelling and Facile Synthesis of a Highly Active Boron-Doped Palladium Catalyst for the Oxygen Reduction Reaction

Tat Thang Vo Doan[+], Jingbo Wang[+], Kee Chun Poon, Desmond C. L. Tan, Bahareh Khezri, Richard D. Webster, Haibin Su, and Hirotaka Sato**

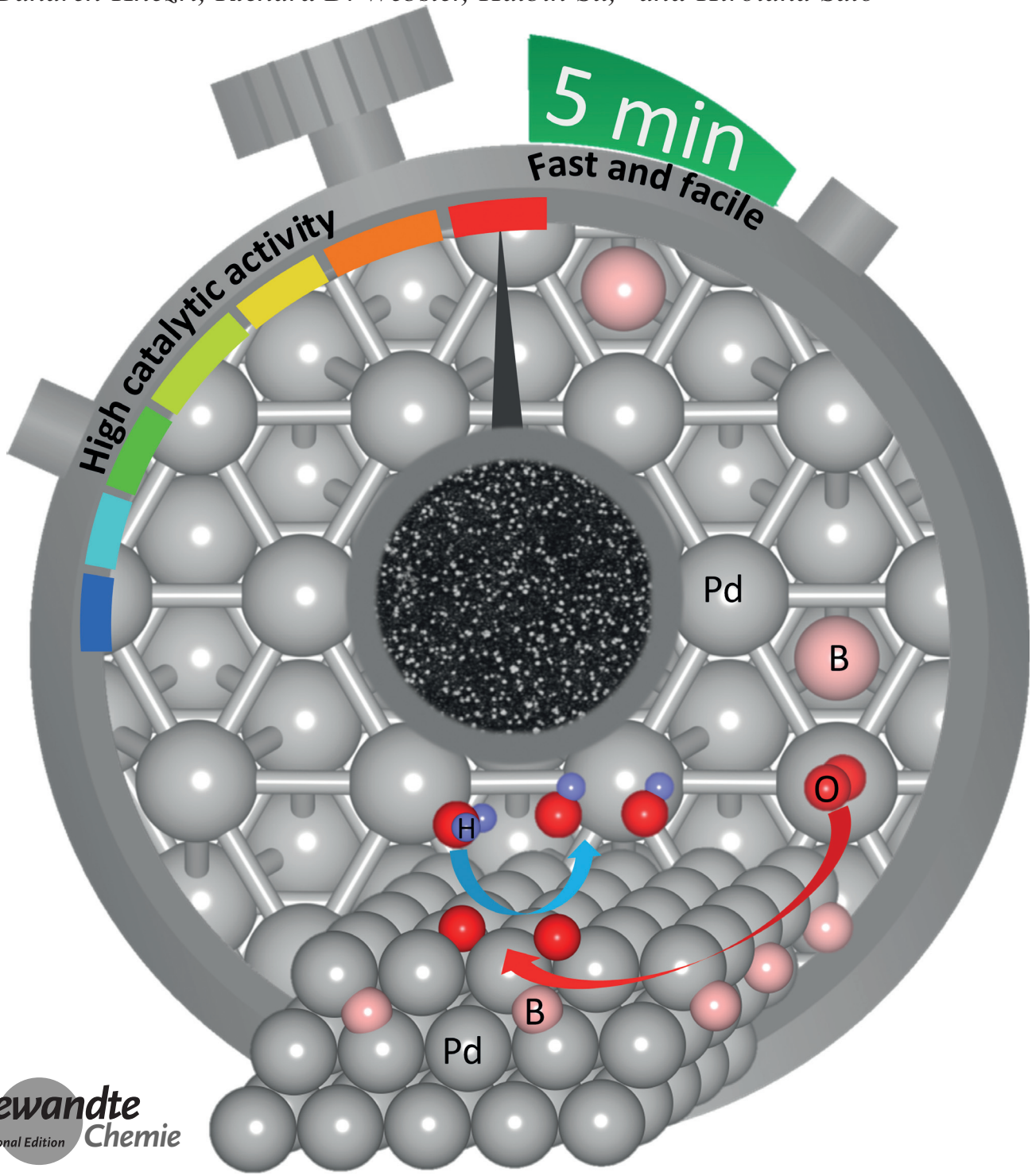

Abstract: *A highly active alternative to Pt electrocatalysts for the oxygen reduction reaction (ORR), which is the cathode-electrode reaction of fuel cells, is sought for higher fuel-cell performance. Our theoretical modelling reveals that B-doped Pd (Pd-B) weakens the absorption of ORR intermediates with nearly optimal binding energy by lowering the barrier associated with O_2 dissociation, suggesting Pd-B should be highly active for ORR. In fact, Pd-B, facile synthesized by an electroless deposition process, exhibits 2.2 times and 8.8 times higher specific activity and 14 times and 35 times less costly than commercial pure Pd and Pt catalysts, respectively. Another computational result is that the surface core level of Pd is negatively shifted by B doping, as confirmed by XPS, and implies that filling the density of states related to the anti-bonding of oxygen to Pd surfaces with excess electrons from B doping, weakens the O bonding to Pd and boosts the catalytic activity.*

In fuel cells, the oxygen reduction reaction (ORR) plays an important role, because oxygen is a common fuel for cathodic reduction. However, the ORR is non-facile because the O=O bond is very strong.[1] Developing highly active oxygen-reduction electrocatalysts at low cost remains a great challenge, although intensive efforts have been expended on the development of cathode materials. Non-precious metal-based catalysts, such as transition-metal nitrogen carbon (M-N-C, M = Co, Fe, Ni, Mn)[2] and transition-metal oxides (MO_x, M = Mn, Fe, Co, Cu,)[3] exhibit high ORR catalytic activity and have drawn much attention owing to their abundance and low cost. Metal-free materials ,such as nitrogen-doped carbon have shown significant improvement in ORR catalytic activity that reaches the level of commercial Pt/C in term of onset potential and half-wave potential.[3d,4] They are very promising catalysts but need further improvement in terms of durability, synthesis process (mostly high vacuum, high temperature, or long synthesis time is required), or electric conductivity.[5] Platinum is thus still the practically used ORR catalyst and platinum-alternative precious-metal catalysts have been intensively investigated.

Nørskov and co-workers established the so-called volcano curve, which relates the oxygen reduction activity of different metals and alloys to the binding energy of atomic oxygen.[1d–f,6] According to these curves, the pure metals Pt and Pd exhibit superior catalytic activities for oxygen reduction, which can be further improved by alloying them with other elements to weaken the oxygen binding strength. This notion has been confirmed by the enhanced ORR activity of Pt_3M alloys (M = Ni, Co, Fe, V, Ti, Sc, Y) in which the d-band center of the Pt atoms is lower than that of pure Pt.[1e,f,6] Pt-alternative catalysts that will lower the cost while maintaining the high ORR activity have also been researched.[7] The activities of Pd-alloy catalysts (Pd–Co and Pd–Fe) are comparable with that of Pt.[7b,c,f] Despite a recent report on P-doped Pd that exhibited very high catalytic activity owing to its amorphous structure,[8] much less work has been devoted to doping non-metallic elements into Pd. In the present study, we seek to understand how the ORR is enhanced in an alloyed catalyst (e.g. B-doped Pd). The investigation combines density functional theory (DFT) calculations[1e,6b,9] with experimental studies. We first investigated the adsorption of ORR intermediates onto the Pd material, constructed the ORR mechanism, and identify the preferential mechanism on the pure Pd and B-doped Pd catalysts. We then synthesized a real B-doped Pd and pure Pd catalyst by our previously developed stepwise electroless deposition process.[8] In this method, the electrode is sequentially dipped into two different solutions, the first containing a reducing agent (in this study, dimethylaminoborane (DMAB) or hydrazine (N_2H_4)) and the second containing a metal salt (metal ion source, $PdCl_2$). During the second dipping, Pd nanoparticles are electrochemically deposited onto the electrode surface. The Pd nanoparticles become doped with B atoms released by the decomposition of DMAB (herein, the B-doped Pd is denoted as Pd–B) while pure Pd is deposited (no doping) when hydrazine is used (the synthesized pure Pd is denoted as Pd–N_2H_4). As predicted by the theoretical modelling, the synthesized Pd–B exhibits superior catalytic activity to the Pd–N_2H_4 and a commercial Pd-loaded carbon (denoted as Pd/C). Finally, to further understand the mechanism of the ORR enhancement in Pd–B, we compute the surface core level shift (SCLS), defined as the difference in core level binding energy between the surface and bulk, for the pure Pd and Pd–B catalysts, and experimentally confirm the computations by X-ray photoelectron spectroscopy (XPS).

The ORR intermediate species (especially the radical species) adsorb more weakly on the surface of Pd–B than on Pd as summarized from Table S1 in the Supporting Information. On the pure Pd surface, O prefers the fcc hollow, that is, the f site with a binding energy of −4.44 eV, whereas on B doped Pd surface (Pd–B), the f_2 site is preferred with a binding energy of −4.12 eV: the B doping weakens the O adsorption by 0.32 eV. According to the work by Stamenkovic et al.,[6b] the highest ORR catalyst is predicted to bind O more weakly than pure Pt by 0.20 eV. Since O adsorbs 0.06 eV more strongly to Pd(111) than to Pt-(111),[7b,10] the downshift should be 0.26 eV (relative to pure Pd) to reach the maximum activity. Therefore, Pd–B exhibits nearly optimal O adsorption and should have high catalytic activity for ORR.

OH and O_2 preferentially bind to the f sites on the pure Pd surface with binding energies of −2.58 eV and −0.99 eV,

[*] T. T. Vo Doan,[+] K. C. Poon, D. C. L. Tan, Prof. H. Sato
School of Mechanical and Aerospace Engineering
Nanyang Technological University
50 Nanyang Avenue, Singapore 639798 (Singapore)
E-mail: hirosato@ntu.edu.sg
J. Wang,[+] Prof. H. Su
School of Materials Science & Engineering
Nanyang Technological University
50 Nanyang Avenue, Singapore 639798 (Singapore)
E-mail: hbsu@ntu.edu.sg
B. Khezri, Prof. R. D. Webster
Division of Chemistry & Biological Chemistry, School of Physical and Mathematical Sciences, Nanyang Technological University
21 Nanyang Link, Singapore 637371 (Singapore)
[+] These authors contributed equally to this work.

Supporting information for this article can be found under: http://dx.doi.org/10.1002/anie.201601727.

respectively. On Pd–B, these binding energies decrease down to −2.55 eV and −0.67 eV, respectively. H_2O always prefers the top site of the Pd surface regardless of B-doping; the directions of the H atoms have little effect on the binding strength. All the above binding energies on the Pd surface are consistent with previous results by DFT calculations.[7a,11]

Furthermore, the binding energies show stronger site-dependence on Pd–B than on pure Pd. Depending on the number of underlying B atoms, the binding strength of O varies from −3.62 eV to −4.12 eV. The variation (0.50 eV) is much wider than the variation on Pd(111) surfaces (0.26 eV). A similar trend is seen for OH adsorption. The energy range of OH adsorption reduces from 0.39 eV on Pd–B to 0.21 eV on Pd(111). Although the adsorption of the saturated species (O_2 and H_2O) is relatively insensitive to site configuration, it remains more variable on Pd–B than on the Pd(111) surface. Since the Pd–B surface contains two distinct preferable adsorption sites for O_2 and O with lower binding energies than for Pd(111), this optimizes both dissociative adsorption of O_2 and further reduction of O similar to the scenario suggested by the simple thermodynamic model proposed by Bard and co-workers.[7f]

Considering the binding energies of the ORR intermediates in the Table S1, we can briefly understand the ORR activity enhancement of the Pd-alloyed B catalysts and implement the reaction barrier calculations for additional insight. The ORR mechanism has been extensively studied on Pt-alloyed and transition-metal surfaces in acidic solutions.[1d,10–12] However, it appears that the reaction scheme in alkaline electrolytes has been largely neglected.[13]

Given that H_2O is a stronger proton donor than OH in alkaline solutions,[12c,13,14] and assuming that all intermediates are adsorbed to the surface, the elementary steps (R1)–(R9) described in Table 1 can be categorized into three possible mechanisms:

I. The dissociative mechanism involves the dissociation of O_2 (R1), followed by the hydration of adsorbed O to OH (R3).
II. The associative mechanism is initiated by the hydration of O_2 to form HO_2 (R2), followed by HO_2 dissociation into OH (R4) or its hydration to H_2O_2 (R5). Finally, OH is formed by H_2O_2 decomposition (R6).
III. Reactions related to direct water dissociation into H and OH (R7), followed by H insertion into O_2 (R8) and HO_2 (R9).

Table 1: Reaction barriers E_a (eV) and reaction energies ΔE (eV) of ORR reactions on B-doped Pd and Pd(111) surfaces.

Reactions		Pd(111)		B-doped Pd (111)	
		E_a	ΔE	E_a	ΔE
(R1)	$O_2 \rightleftharpoons 2O$	0.72	−1.46	0.63	−1.18
(R2)	$O_2 + H_2O \rightleftharpoons HO_2 + OH$	0.68	0.65	0.71	0.64
(R3)	$O + H_2O \rightleftharpoons OH + OH$	0.37	0.27	0.17	0.02
(R4)	$HO_2 \rightleftharpoons OH + O$	0.02	−1.84	0.08	−1.58
(R5)	$HO_2 + H_2O \rightleftharpoons H_2O_2 + OH$	0.65	0.56	0.56	0.41
(R6)	$H_2O_2 \rightleftharpoons 2OH$	0.20	−2.32	0.19	−1.74
(R7)	$H_2O \rightleftharpoons H + OH$	1.03	0.35	1.22	0.42
(R8)	$O_2 + H \rightleftharpoons HO_2$	0.68	0.01	0.55	−0.26
(R9)	$HO_2 + H \rightleftharpoons H_2O_2$	0.43	−0.25	0.62	−0.29

The primary factor determining which mechanism prevailing is the relative feasibility of the rate-determining step among above mechanisms. For each type of mechanism, the initiation reaction corresponds to the rate-determining step. In mechanisms I, II, and III, the initiation reactions are step (R1), the O_2 dissociation, step (R2), the hydration of O_2 to HO_2 and step (R7), direct dissociation of H_2O, respectively. Because water dissociation must overcome a higher barrier (>1 eV) than the other steps, mechanism III cannot occur on both surfaces. The barriers of R8 and R9 on Pd(111) are 0.68 and 0.43 eV, respectively, consistent with those of previous results.[10,11] On Pd(111), the barrier of R1 is slightly higher than that of R2 (0.72 eV vs. 0.68 eV). Because these two rate-determining steps are very similar on the Pd(111) surface, the dissociative and associative mechanisms compete, although the associative mechanism is slightly more dominant. This situation alters on the Pd–B surface, where the barrier difference between R1 and R2 (0.63 eV vs. 0.71 eV) becomes sufficiently wide that the dissociative mechanism dominates. From the rate-determining step of the preferential mechanism, we can estimate the ORR activity of Pd-B and compare it with that of pure Pd. The comparison predicts a seven-fold

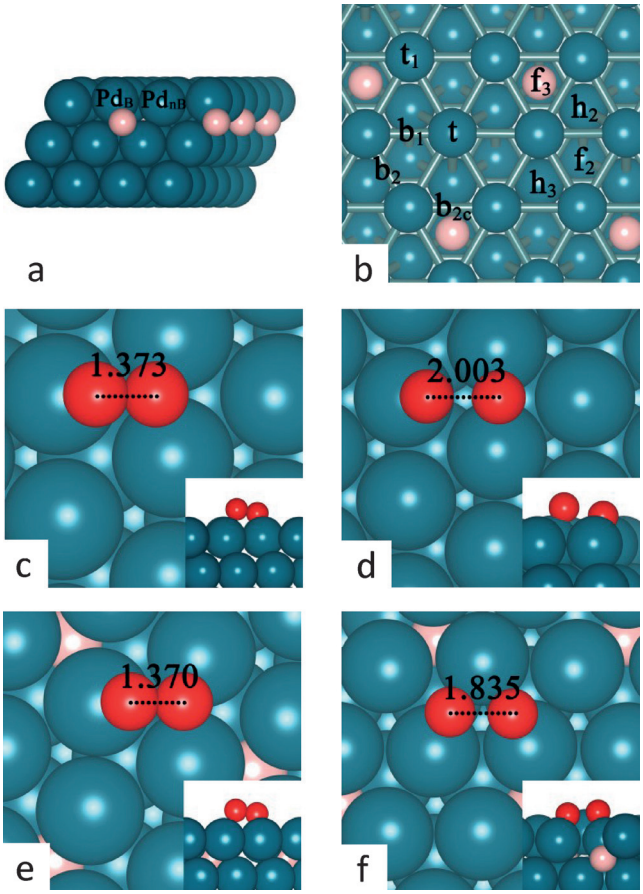

Figure 1. B-doped Pd surface and the reaction path of O_2 dissociation. a),b) Side view (a) and top view (b) of the Pd–B surface. The configurations of the Pd atoms and binding site notations are explained in the footnote of Table S1. c)–f) Two adjacent images represent a path on a surface, c),d) on Pd(111) and e),f) on Pd–B. c) and e) show the structure of the reactant and d) and f) show the geometry of the transition state. Pd cyan, B pink, O red.

increase in the catalytic activity of Pd–B relative to pure Pd at 25 °C ($e^{-\frac{0.63e\ V}{kT}}/e^{-\frac{0.68e\ V}{kT}} = 7$). Considering the slowdown on Pd(111) by the competitive mechanism I, B-doping of the Pd should accelerate the reaction kinetics by an order of magnitude.

From a thermodynamic viewpoint, the higher binding energies of the reactant should lower the dissociation barrier.[10,16] However, O_2 dissociation proceeds with a smaller barrier on Pd–B than on Pd (0.63 eV vs. 0.72 eV), for reasons that require further investigation. In the initial state, the O–O distance on Pd–B is 1.370 Å (Figure 1e), 0.003 Å shorter than on Pd(111) (Figure 1c). This implies that O_2 interacts more strongly with pure Pd than with Pd–B.

From the reactant to transition states, the O–O bond is elongated by 0.630 Å on the Pd surface but by only 0.462 Å on the Pd–B surface. This shorter elongation implies that the transition state occurs earlier on Pd–B than that on Pd, thus the barrier is reduced on Pd–B and kinetically facilitating the dissociative adsorption of O_2.

According to the above-described theoretical model, B-doped Pd nanoparticles should exhibit higher catalytic ORR activity than pure Pd nanoparticles. We now evaluate this activity using B-doped Pd nanoparticles synthesized by a previously developed stepwise electroless deposition process.[8] In this process, a glassy carbon electrode is sequentially dipped into two separate solutions, one containing DMAB (reducing agent, the source of B), and the other containing $PdCl_2$ (Pd ion source). Each dipping is held for a specified time (see the supporting information for details). This deposition process formed well-dispersed crystalline Pd nanoparticles (Figure 2a and Figure S1). Boron was actually co-deposited on the Pd nanoparticles during the electroless deposition, as evidenced by the Inductively coupled plasma mass spectrometry (ICP-MS) data of the obtained Pd nanoparticles (B content = 11.8 ± 0.7 at%). Furthermore, the XRD profile supports the fact that the co-deposited B is indeed embedded in the Pd lattice (Figure 2b). Every peak in the Pd–B profile shifts to a lower angle than in the Pd–N_2H_4, Pd/C, and pure Pd bulk profiles, suggesting that the Pd lattice has expanded due to the B doping as also confirmed by HR-TEM images (Figure S1).

As predicted by the theoretical model, the synthesized Pd–B nanoparticles catalyst indeed exhibits higher catalytic activity than Pd/C (Figure 3a; Table 2). The positive half-wave potential (0.86 V) is higher in the B-doped Pd particle catalyst than in Pd–N_2H_4 (0.83 V) and Pd/C (0.83 V). The specific activity of the B-doped Pd particles (4.13 mA cm^{-2}), defined as the kinetic current normalized by the electrochemical active surface area (ECSA), is over 1.4 times, 2.5 times, and 8.8 times higher than those of Pd–N_2H_4, Pd/C and Pt/C, respectively (Table 2). Moreover, the mass activity, defined as the kinetic current normalized by the Pd load, is 1.7 times, 14 times, and 35 times higher in the B-doped Pd nanoparticles than those of Pd–N_2H_4, Pd/C, and Pt/C,

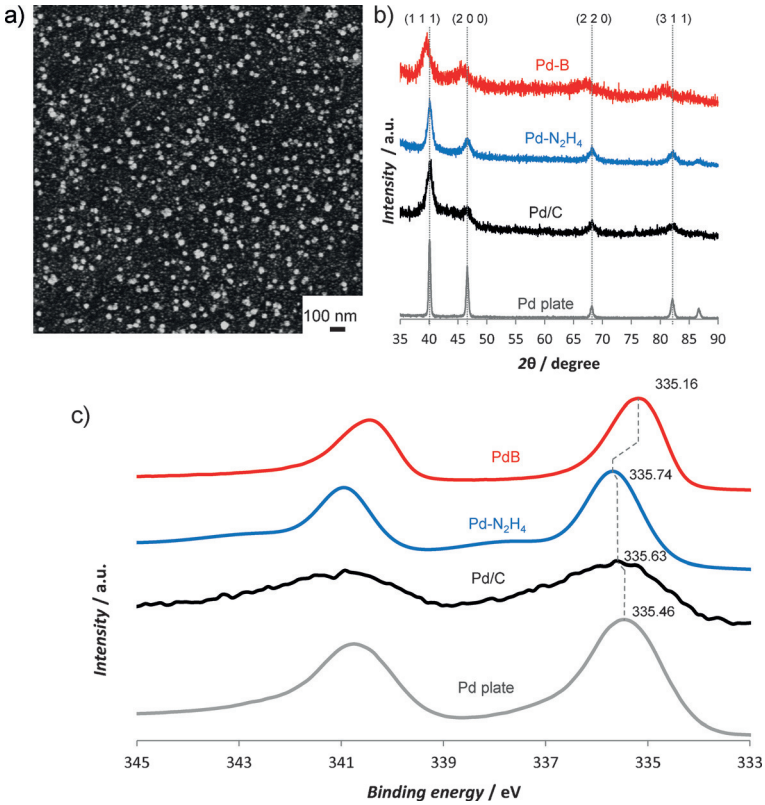

Figure 2. Physical properties of B-doped Pd (Pd–B) nanoparticles. a) Field emission scanning electron microscopy image of Pd–B nanoparticles. b) X-ray diffraction (XRD) patterns, and c) X-ray photoelectron spectra (XPS) of Pd–B, Pd–N_2H_4, commercial Pd/C, and Pd plate. The calibration for XPS was carried out using C1s binding energy at 284.5 eV.[15] Gray dotted lines in (b) and (c) indicate the position/change in position of a peak relative to its position in the trace of Pd plate.

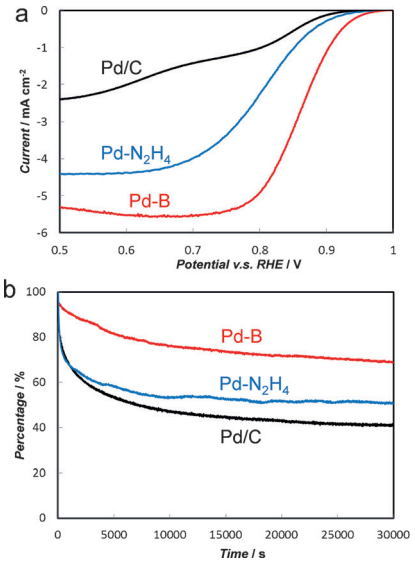

Figure 3. Electrochemical performances of ORR catalysts, Pd–B, Pd–N_2H_4, and Pd/C nanoparticles. a) ORR polarization curves were measured in 0.1 M O_2-saturated KOH solution at a scan rate of 10 mV s^{-1}. Rotational speed: 1600 rpm.[8,19] b) Chronoamperometry responses were evaluated as percentage of initial current density. The measurements were performed in 0.1 M O_2-saturated KOH solution at a potential of 0.67 V versus the reversible hydrogen electrode (RHE). Rotational speed: 200 rpm.[8,20]

Table 2: Half-wave potentials and specific and mass activities of Pd and Pt catalysts.[a]

Catalyst	Half-wave potential [V]	Specific activity [mA cm^{-2}]	Mass activity [mA μg^{-1}]
Pd–B	0.86	4.13	2.38
Pd–N_2H_4[8]	0.83	2.87	1.33
Pd/C[8]	0.83	1.58	0.17
Pt/C[8]	0.74	0.47	0.068

[a] Specific and mass activities were calculated as described elsewhere. The current was measured at 0.85 V vs. RHE at a rotational speed of 1600 rpm. The values are averaged from several experiments.[8,19a]

respectively. Considering the market price of Pd is lower than that of Pt,[17] Pd–B catalyst is more than 35 times less costly than Pt. The high catalytic activity of Pd–B is also maintained over a long time. In the durability test, Pd–B maintained over 75% of its initial catalytic activity, whereas the catalytic activity of Pd–N_2H_4 and Pd/C rapidly reduced to 53% and 47%, respectively, within 10000 s (Figure 3b).

On the modelled Pd–B surface, Pd atoms are either directly bonded to B atoms or have no B neighbors. In Figure 1a,b, these two situations are labelled Pd_B and Pd_{nB}, respectively. Table S2 lists the surface core level shifts (SCLSs) of the Pd atoms in each case for the upper two layers of Pd–B together with the results for Pd(111). Boron-doping dramatically changes the SCLSs of the Pd_B state in both layers. In fact, the SCLSs switch sign, changing to 0.07 and 0.16 eV from −0.46 and −0.28 eV in the top and second layers of Pd(111), respectively. In contrast, the SCLS of Pd_{nB} scarcely changes from that of Pd(111) in the first layer but becomes more negative in the second layer. Considering the connection between the core level shift and charge transfer,[18] we conclude that the Pd_B atoms in the top two layers lose electrons. Consequently, the electron density increases around B and Pd_{nB} atoms in the second layer. This conclusion is supported by the experimental XPS results of the synthesized Pd–B nanoparticles (Figure 2c). Since the B composition in the nanoparticles is 12 at%, most of the Pd atoms in the nanoparticles are the type of Pd_{nB}, as reflected in the XPS profile of Pd–B. The binding energy of Pd–B is lowered relative to pure Pd (Figure 2c), consistent with the computational results. Again, most of the surface atoms of the synthesized Pd–B nanoparticles exhibit higher electron density than those observed in the pure Pd nanoparticles. Such excess electrons would effectively weaken the bonding between O and Pd atoms, reducing the binding energy (Table S1) and boosting the catalytic activity of Pd–B (Table 1, Figure 3).

In conclusion, a B-doped Pd catalyst is successfully developed and exhibits superior catalytic activity to undoped Pd catalysts. This was made possible by characterizing the ORR mechanisms on the pure Pd and B-doped Pd surfaces (the difference between B-doped Pd and amorphous P-doped Pd[8] is discussed in the Supporting Information). The doping of B on the Pd surface reduces the binding strengths of the ORR intermediates. Oxygen adsorption in the B-doped Pd catalyst was reduced by 0.32 eV, implying that the activity of this catalyst is nearly optimal. The ORR activity on the B-doped Pd catalyst is enhanced by the large site dependence of the binding energy. According to the mechanistic analysis, the B-doped Pd surface presents a lower barrier to O_2 dissociation than pure Pd, suggesting better catalytic activity of Pd–B than pure Pd. In fact, in terms of the half-wave potential, specific and mass activities, and durability, the catalytic activity of the synthesized Pd–B nanoparticles is superior to the pure Pd. In addition, as determined from the modelled B-doped Pd surface and the experimental XPS data of the synthesized Pd–B, the SCLS becomes positive when Pd atoms bond to B, implying electron transfer from Pd to B atoms. Such additional electrons on the Pd–B surface would improve the catalytic activity. Notably, the stepwise electroless deposition (by which we synthesized the Pd–B) is remarkably facile, requires no harsh conditions (high temperature and vacuum)- and is completed within a short time (in the present study, the total synthesis time was less than 5 min). In addition, by changing the metal-ion source and reducing agent, we can synthesize a variety of pure metal and alloy catalysts with different microstructures.[8] The stepwise electroless deposition is suitable for rational tailoring and design of catalyst materials.

Acknowledgements

This study was financially supported by the Nanyang Assistant Professorship (NAP, M4080740) and Singapore Ministry of Education (MOE2013-T2-2-049). We appreciate Ms. Koh Joo Luang, Ms. Yong Mei Yoke, Mr. Leong Kwok Phui, and Ms. Lee Pui Mun at Material/Biological & Chemical Laboratories at MAE, NTU, for their continuous support and effort to set up and maintain an excellent experimental environment. We thank Dr. Ming Lin at IMRE, A*STAR, for his help in obtaining the HR-TEM images.

Keywords: density functional theory · electrocatalysts · nanoparticles · oxygen reduction reaction · palladium

How to cite: *Angew. Chem. Int. Ed.* **2016**, *55*, 6842–6847
Angew. Chem. **2016**, *128*, 6956–6961

[1] a) N. M. Marković, T. J. Schmidt, V. Stamenković, P. N. Ross, *Fuel Cells* **2001**, *1*, 105–116; b) H. A. Gasteiger, S. S. Kocha, B. Sompalli, F. T. Wagner, *Appl. Catal. B* **2005**, *56*, 9–35; c) A. A. Gewirth, M. S. Thorum, *Inorg. Chem.* **2010**, *49*, 3557–3566; d) J. K. Nørskov, J. Rossmeisl, A. Logadottir, L. Lindqvist, J. R. Kitchin, T. Bligaard, H. Jónsson, *J. Phys. Chem. B* **2004**, *108*, 17886–17892; e) J. Greeley, I. E. L. Stephens, A. S. Bondarenko, T. P. Johansson, H. A. Hansen, T. F. Jaramillo, J. Rossmeisl, I. Chorkendorff, J. K. Nørskov, *Nat. Chem.* **2009**, *1*, 552–556; f) V. R. Stamenkovic, B. S. Mun, M. Arenz, K. J. J. Mayrhofer, C. A. Lucas, G. Wang, P. N. Ross, N. M. Markovic, *Nat. Mater.* **2007**, *6*, 241–247.

[2] a) E. Yeager, *Electrochim. Acta* **1984**, *29*, 1527–1537; b) H. Liu, C. Song, Y. Tang, J. Zhang, J. Zhang, *Electrochim. Acta* **2007**, *52*, 4532–4538; c) H.-W. Liang, W. Wei, Z.-S. Wu, X. Feng, K. Müllen, *J. Am. Chem. Soc.* **2013**, *135*, 16002–16005; d) M. Lefèvre, E. Proietti, F. Jaouen, J.-P. Dodelet, *Science* **2009**, *324*, 71–74; e) S. Kattel, G. Wang, *J. Phys. Chem. Lett.* **2014**, *5*, 452–

456; f) Y. Hu, J. O. Jensen, W. Zhang, L. N. Cleemann, W. Xing, N. J. Bjerrum, Q. Li, *Angew. Chem. Int. Ed.* **2014**, *53*, 3675 – 3679; *Angew. Chem.* **2014**, *126*, 3749 – 3753.

[3] a) H. Zhu, S. Zhang, Y.-X. Huang, L. Wu, S. Sun, *Nano Lett.* **2013**, *13*, 2947 – 2951; b) Y. Zhang, Y. Hu, S. Li, J. Sun, B. Hou, *J. Power Sources* **2011**, *196*, 9284 – 9289; c) Q. Shi, F. Peng, S. Liao, H. Wang, H. Yu, Z. Liu, B. Zhang, D. Su, *J. Mater. Chem. A* **2013**, *1*, 14853 – 14857; d) Y. Liang et al., *J. Am. Chem. Soc.* **2012**, *134*, 15849 – 15857; e) F. Cheng, T. Zhang, Y. Zhang, J. Du, X. Han, J. Chen, *Angew. Chem. Int. Ed.* **2013**, *52*, 2474 – 2477; *Angew. Chem.* **2013**, *125*, 2534 – 2537.

[4] a) Y. Zheng, Y. Jiao, L. Ge, M. Jaroniec, S. Z. Qiao, *Angew. Chem. Int. Ed.* **2013**, *52*, 3110 – 3116; *Angew. Chem.* **2013**, *125*, 3192 – 3198; b) C. H. A. Wong, C. K. Chua, B. Khezri, R. D. Webster, M. Pumera, *Angew. Chem. Int. Ed.* **2013**, *52*, 8685 – 8688; *Angew. Chem.* **2013**, *125*, 8847 – 8850; c) P. Su, H. Xiao, J. Zhao, Y. Yao, Z. Shao, C. Li, Q. Yang, *Chem. Sci.* **2013**, *4*, 2941 – 2946; d) R. Liu, D. Wu, X. Feng, K. Müllen, *Angew. Chem. Int. Ed.* **2010**, *49*, 2565 – 2569; *Angew. Chem.* **2010**, *122*, 2619 – 2623; e) W. Ding et al., *Angew. Chem. Int. Ed.* **2013**, *52*, 11755 – 11759; *Angew. Chem.* **2013**, *125*, 11971 – 11975; f) P. Chen, L.-K. Wang, G. Wang, M.-R. Gao, J. Ge, W.-J. Yuan, Y.-H. Shen, A.-J. Xie, S.-H. Yu, *Energy Environ. Sci.* **2014**, *7*, 4095 – 4103.

[5] a) Y. Nie, L. Li, Z. Wei, *Chem. Soc. Rev.* **2015**, *44*, 2168 – 2201; b) X. Ge, A. Sumboja, D. Wuu, T. An, B. Li, F. W. T. Goh, T. S. A. Hor, Y. Zong, Z. Liu, *ACS Catal.* **2015**, *5*, 4643 – 4667.

[6] a) V. Stamenkovic, B. S. Mun, K. J. J. Mayrhofer, P. N. Ross, N. M. Markovic, J. Rossmeisl, J. Greeley, J. K. Nørskov, *Angew. Chem. Int. Ed.* **2006**, *45*, 2897 – 2901; *Angew. Chem.* **2006**, *118*, 2963 – 2967; b) V. R. Stamenkovic, B. Fowler, B. S. Mun, G. Wang, P. N. Ross, C. A. Lucas, N. M. Marković, *Science* **2007**, *315*, 493 – 497.

[7] a) L. Xiao, L. Zhuang, Y. Liu, J. Lu, H. D. Abruña, *J. Am. Chem. Soc.* **2009**, *131*, 602 – 608; b) Y. Suo, L. Zhuang, J. Lu, *Angew. Chem. Int. Ed.* **2007**, *46*, 2862 – 2864; *Angew. Chem.* **2007**, *119*, 2920 – 2922; c) M. Shao, P. Liu, J. Zhang, R. Adzic, *J. Phys. Chem. B* **2007**, *111*, 6772 – 6775; d) Y. Liang, Y. Li, H. Wang, J. Zhou, J. Wang, T. Regier, H. Dai, *Nat. Mater.* **2011**, *10*, 780 – 786; e) Y. Li, W. Zhou, H. Wang, L. Xie, Y. Liang, F. Wei, J.-C. Idrobo, S. J. Pennycook, H. Dai, *Nat. Nanotechnol.* **2012**, *7*, 394 – 400; f) J. L. Fernández, D. A. Walsh, A. J. Bard, *J. Am. Chem. Soc.* **2005**, *127*, 357 – 365.

[8] K. C. Poon, D. C. L. Tan, T. D. T. Vo, B. Khezri, H. Su, R. D. Webster, H. Sato, *J. Am. Chem. Soc.* **2014**, *136*, 5217 – 5220.

[9] J. K. Nørskov, T. Bligaard, J. Rossmeisl, C. H. Christensen, *Nat. Chem.* **2009**, *1*, 37 – 46.

[10] D. C. Ford, A. U. Nilekar, Y. Xu, M. Mavrikakis, *Surf. Sci.* **2010**, *604*, 1565 – 1575.

[11] P. Tian, L. Ouyang, X. Xu, J. Xu, Y.-F. Han, *Chin. J. Catal.* **2013**, *34*, 1002 – 1012.

[12] a) H.-C. Tsai, T. H. Yu, Y. Sha, B. V. Merinov, P.-W. Wu, S.-Y. Chen, W. A. Goddard, *J. Phys. Chem. C* **2014**, *118*, 26703 – 26712; b) T. Toda, H. Igarashi, H. Uchida, M. Watanabe, *J. Electrochem. Soc.* **1999**, *146*, 3750 – 3756; c) V. Tripković, E. Skúlason, S. Siahrostami, J. K. Nørskov, J. Rossmeisl, *Electrochim. Acta* **2010**, *55*, 7975 – 7981; d) A. B. Anderson, T. V. Albu, *J. Electrochem. Soc.* **2000**, *147*, 4229 – 4238; e) T. H. Yu, T. Hofmann, Y. Sha, B. V. Merinov, D. J. Myers, C. Heske, W. A. Goddard, *J. Phys. Chem. C* **2013**, *117*, 26598 – 26607.

[13] T. J. Schmidt, V. Stamenkovic, M. Arenz, N. M. Markovic, P. N. Ross, Jr., *Electrochim. Acta* **2002**, *47*, 3765 – 3776.

[14] G. S. Karlberg, G. Wahnström, *J. Chem. Phys.* **2005**, *122*, 194705.

[15] a) J. C. Bertolini, P. Delichere, B. C. Khanra, J. Massardier, C. Noupa, B. Tardy, *Catal. Lett.* **1990**, *6*, 215 – 223; b) K. Noack, H. Zbinden, R. Schlögl, *Catal. Lett.* **1990**, *4*, 145 – 155; c) W. Zhou, M. Li, O. L. Ding, S. H. Chan, L. Zhang, Y. Xue, *Int. J. Hydrogen Energy* **2014**, *39*, 6433 – 6442.

[16] Y.-H. Zhao, K. Sun, X. Ma, J. Liu, D. Sun, H.-Y. Su, W.-X. Li, *Angew. Chem. Int. Ed.* **2011**, *50*, 5335 – 5338; *Angew. Chem.* **2011**, *123*, 5447 – 5450.

[17] a) P. C. K. Vesborg, T. F. Jaramillo, *RSC Adv.* **2012**, *2*, 7933 – 7947; b) ScotiaMocatta, *Precious Metals 2016 Forecast—PGM* **2015**; c) Johnson Matthey plc, *PGM Market Report*, May 2015; d) A. Cowley, *Platinum Met. Rev.* **2013**, *57*, 215 – 216.

[18] a) J. A. Rodriguez, D. W. Goodman, *Science* **1992**, *257*, 897 – 903; b) M. Methfessel, V. Fiorentini, S. Oppo, *Phys. Rev. B* **2000**, *61*, 5229 – 5236.

[19] a) M. H. Seo, S. M. Choi, H. J. Kim, W. B. Kim, *Electrochem. Commun.* **2011**, *13*, 182 – 185; b) L. Jiang, A. Hsu, D. Chu, R. Chen, *J. Electrochem. Soc.* **2009**, *156*, B643 – B649.

[20] S. Guo, S. Zhang, L. Wu, S. Sun, *Angew. Chem. Int. Ed.* **2012**, *51*, 11770 – 11773; *Angew. Chem.* **2012**, *124*, 11940 – 11943.

Received: February 18, 2016
Revised: March 21, 2016
Published online: April 15, 2016

